ORIGINAL ARTICLE

Effect of the dynamical collision frequency on quantum wakefields

Zh.A. Moldabekov[1,2] | **S.M. Amirov**[2] | **P. Ludwig**[1] | **M. Bonitz**[1] | **T.S. Ramazanov**[2]

[1]Institut für Theoretische Physik und Astrophysik, Christian-Albrechts-Universität zu Kiel, Kiel, Germany

[2]Institute for Experimental and Theoretical Physics, Al-Farabi Kazakh National University, Almaty, Kazakhstan

* Correspondence
Zh.A. Moldabekov, Institut für Theoretische Physik und Astrophysik, Christian-Albrechts-Universität zu Kiel Leibnizstraße 15, Kiel, Germany.
Email: zhandos@physics.kz

Previous papers on the quantum wakefield around an ion moving in a dense plasma have considered the collision frequency in the static approximation. In this work, we present the results of the dynamically screened ion potential taking into account the dynamical electron–ion collision frequency. The Lenard–Balescu dynamical collision frequency and various approximations to it are considered. As a main result of our investigation for the subsonic, sonic, and supersonic regimes, we find that the frequency dependence of collisions can be safely discarded if the electronic streaming velocity (relative to an ion) is comparable to or less than the electronic Fermi velocity.

KEYWORDS

dense plasmas, dynamical collision frequency, dynamical screening, Lenard–Balescu approximation, quantum wakefield

1 | INTRODUCTION

Electrons streaming relative to ions can appear in plasmas as a result of the impact by electron (ion) beams and electron acceleration by lasers.[1,2] In our previous works,[3–5] we have studied the wakefield created by streaming electrons around an (immobile) ion by using the Mermin dynamical quantum dielectric function in relaxation time approximation.[6] We extensively investigated different plasma parameters (densities, temperatures) and streaming velocities. The results clearly showed a significant deviation of the potential and the electronic density distribution from those of the corresponding equilibrium case.[3] The common features and differences between the wakefield (dynamically screened ion potential) in dense quantum plasmas, in classical complex (dusty) plasmas,[7–9] and in ultra-relativistic quark-gluon plasmas have been analysed in ref. [4]. The peculiar non-monotonic dependence of the dynamically screened ion potential was reported in ref. [5].

In all the mentioned studies, a *static* collision frequency of electrons was used. However, it has been shown that taking into account the frequency dependence of the electron–ion (e–i) collision frequency is crucial for the description of the transport and optical properties of dense plasmas and warm dense matter.[10–14] Therefore, in this paper, we extend our analysis of the wakefield in dense plasmas by implementing the Lenard–Balescu (LB) dynamical collision frequency.[15] Often, the LB approach has been used with additional simplifications.[16–18] In this work, we also implement these approximations to assess their applicability for the computation of the dynamically screened ion potential.

As an ansatz, we compute the dynamically screened ion potential in the framework of linear response theory as[19]

$$\Phi(\vec{r}) = \int \frac{d^3 k}{2\pi^2} \frac{Q_i}{k^2 \varepsilon(\vec{k}, \vec{k} \cdot \vec{u}_e)} e^{i\vec{k}\cdot\vec{r}}, \tag{1}$$

where $Q_i = Z_i |e|$ is the charge of an ion, $\mathbf{u}_e$ is the constant streaming velocity of electrons relative to an ion, and ε is the electronic dielectric function. For the computation of the 3D Fourier transformation, we used an adapted version of the code `Kielstream`.[20] The latter was originally designed for the calculation of the dynamically screened potential in classical complex plasmas. For the case under consideration, `Kielstream` has been modified by implementing the dynamic dielectric function of quantum electrons and by changing the characteristic length and energy scales.

The state of the electronic component of dense plasmas is entirely defined by the degeneracy parameter $\theta = k_B T / E_F$, i.e. the ratio of the characteristic electronic thermal energy ($\beta^{-1} = k_B T$) to the Fermi energy, as well as by the density parameter $r_s = a/a_B$, where a is the mean inter-particle distance and a_B is the first Bohr radius. In addition, we use the streaming parameter $M = u_e/u_F$, where u_F is the Fermi velocity.

2 | MERMIN DIELECTRIC FUNCTION WITH DYNAMICAL COLLISION FREQUENCY

Going beyond the static relaxation time approximation, dynamical electronic collision effects are included in the Mermin dielectric function[15]:

$$\varepsilon_M(\vec{k}, \omega) = 1 + \frac{(\omega + i\nu(\omega))[\varepsilon_{RPA}(\vec{k}, \omega + i\nu(\omega)) - 1]}{\omega + i\nu(\omega)[\varepsilon_{RPA}(\vec{k}, \omega + i\nu(\omega)) - 1]/[\varepsilon_{RPA}(\vec{k}, 0) - 1]}, \tag{2}$$

where $\nu(\omega) = \nu_{ei}(\omega) + \nu_{ee}(\omega)$ denotes the dynamical electron collision frequency, with ν_{ei} and ν_{ee} being the contributions due to e–i and electron–electron (e–e) collisions, respectively. In Equation (2), $\varepsilon_{RPA}(\vec{k}, \omega)$ is the Lindhard dielectric function,[21] i.e. the dielectric function in the random phase approximation (RPA).

First, let us discuss the e–i collision frequency. The LB dynamical e–i collision frequency reads[15]

$$\nu_{ei}^{LB}(\omega) = i\frac{\varepsilon_0 n_i \Omega_0^2}{6\pi^2 e^2 n_e m_e} \int_0^\infty dk k^6 \widetilde{\phi}_{ei}^2(k) S_i(k) \times \frac{1}{\omega}[\varepsilon_{RPA}^{-1}(k, \omega) - \varepsilon_{RPA}^{-1}(k, 0)], \tag{3}$$

where $\widetilde{\phi}_{ei}(k) = -Z_i e^2/(\varepsilon_0 \Omega_0 k^2)$, and $S_i(k)$ is the ionic static structure factor. The latter can be taken from the solution of the Ornstein–Zernike equation or from molecular dynamics (MD) simulations.[22] Equation (3) can be obtained by solving the quantum LB kinetic equation using the energy-dependent relaxation time approximation.[23]

Equation (3) has a strong non-monotonic behaviour around $\omega \approx \omega_p$, which requires careful calculations with very high resolution. However, for the description of the plasma properties, this feature usually can be safely neglected and replaced by the monotonically behaving ω dependence,[11–14] see discussion below. Therefore, to facilitate the calculation of the dynamical collision frequency, a *statically screened* dynamical collision frequency is often used[11–14]:

$$\nu_{ei}^{RPA}(\omega) = -\frac{i}{\omega} \frac{\varepsilon_0 n_i \Omega_0^2}{6\pi^2 e^2 n_e m_e} \int_0^\infty dk k^6 \widetilde{\Phi}_{RPA}^2(k) S_i(k) \times [\varepsilon_{RPA}(k, \omega) - \varepsilon_{RPA}(k, 0)], \tag{4}$$

where $\widetilde{\Phi}_{RPA}(k) = \phi_{ei}(k)\varepsilon_{RPA}^{-1}(k, 0)$ is the statically screened e–i interaction potential with the electronic screening in the RPA. Equation (4) was obtained from Equation (3) by assuming that[16] $\varepsilon_{RPA}^{-1}(k, \omega) \approx [Re\, \varepsilon_{RPA}(k, \omega) - iIm\, \varepsilon_{RPA}(k, \omega)]/[Re\, \varepsilon_{RPA}(k, 0)]^2$, meaning $|Re\, \varepsilon_{RPA}(k, \omega)|^2 \gg |Im\, \varepsilon_{RPA}(k, \omega)|^2$.

Furthermore, often the statically screened potential $\widetilde{\Phi}_{RPA}(k)$ is approximated by the Yukawa potential $\widetilde{\Phi}_Y(k) = -Z_i e^2/[\varepsilon_0 \Omega_0 (k^2 + k_Y^2)]$, which is obtained using the long-wavelength result $\varepsilon_{RPA}^{-1}(k, 0) \approx \varepsilon_{RPA}^{-1}(k \to 0, 0) = k^2/(k^2 + k_Y^2)$,[24] where the Yukawa screening length is defined by the relation $k_Y^2 = \frac{1}{2}k_{TF}^2 \theta^{1/2} I_{-1/2}(\mu/k_B T_e)$. Here, $I_{-1/2}$ is the Fermi integral of order $-1/2$, $k_{TF} = \sqrt{3}\omega_p/v_F$ is the Thomas–Fermi wave number, and μ is the chemical potential of ideal electrons. Implementing the long-wavelength approximation for the statically screened (Yukawa) potential, one can find[11,12,14,16]

$$\nu_{ei}^Y(\omega) = \frac{i}{\omega} \frac{n_i}{6\pi^2 \varepsilon_0 n_e m_e} \int_0^\infty dk k^6 \frac{Z_i^2 e^2}{(k^2 + k_Y^2)^2} S_i(k) \times [\varepsilon_{RPA}(k, \omega) - \varepsilon_{RPA}(k, 0)]. \tag{5}$$

In general, in dense plasmas, the ionic structure leads to slightly lower value of the e–i collision frequency and less pronounced non-monotonic behaviour close to $\omega \approx \omega_p$.[25] In this work, we are not further interested in the effect of $S_i(k)$ on ν_{ei}. Therefore, we take $S_i(k) = 1$. Moreover, as the aim of this study is to explore the effect of the dynamical collision frequency on the plasma wakefield, without loss of generality, we set $Z_i = 1$.

Figures 1 and 2a show the LB collison frequency, $\nu_{ei}(\omega)$, and simplifications based on the statically screened RPA and Yukawa potentials, corresponding to Equations (3)–(5), respectively. Specifically, Figure 1 illustrates the numerical integration of $\nu_{ei}(\omega)$ by means of two independent codes – a C++ code and a Mathematica[26] program for the above-mentioned approximations. Additionally, in Figure 2a comparisons of our calculations with the results by Fortmann et al.[17] are shown, which are in good agreement.

Comparing Figures 1a,b, it can be deduced that the absolute value, of both the real and imaginary parts, of ν_{ei} decreases with increase in temperature θ at a constant density $r_s = 1.0$. In addition, ν_{ei} decreases with increase in density, see Figure 2a. It should be stressed that the non-monotonic feature of ν_{ei}^{LB} around $\omega \approx \omega_p$, as seen in Figure 1, is absent in the case of ν_{ei}^Y and ν_{ei}^{RPA}. Moreover, Figure 1 clearly shows that ν_{ei}^Y underestimates the value of the real part of the e–i collision frequency in comparison
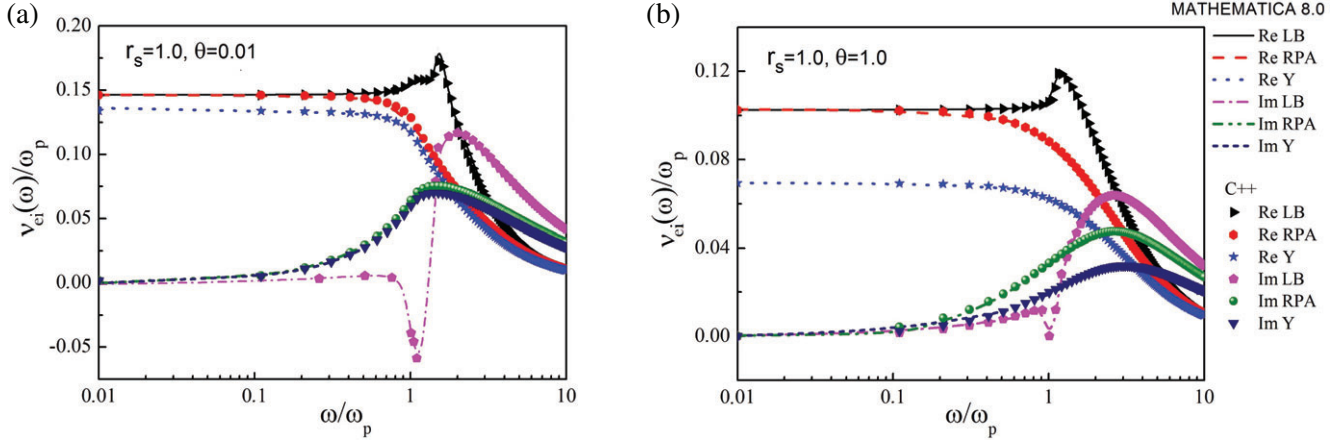
FIGURE 1 Real and imaginary part of the electron–ion dynamical collision frequency at (a) $\theta = 0.01$ and (b) $\theta = 1.0$, where Lenard–Balescu (LB) refers to Equation (3), random phase approximation (RPA) to Equation (4), and Y to Equation (5), respectively. For comparison, two independent numerical implementations with C++ (lines) and Mathematica (symbols) are given. The legend applies to both figures
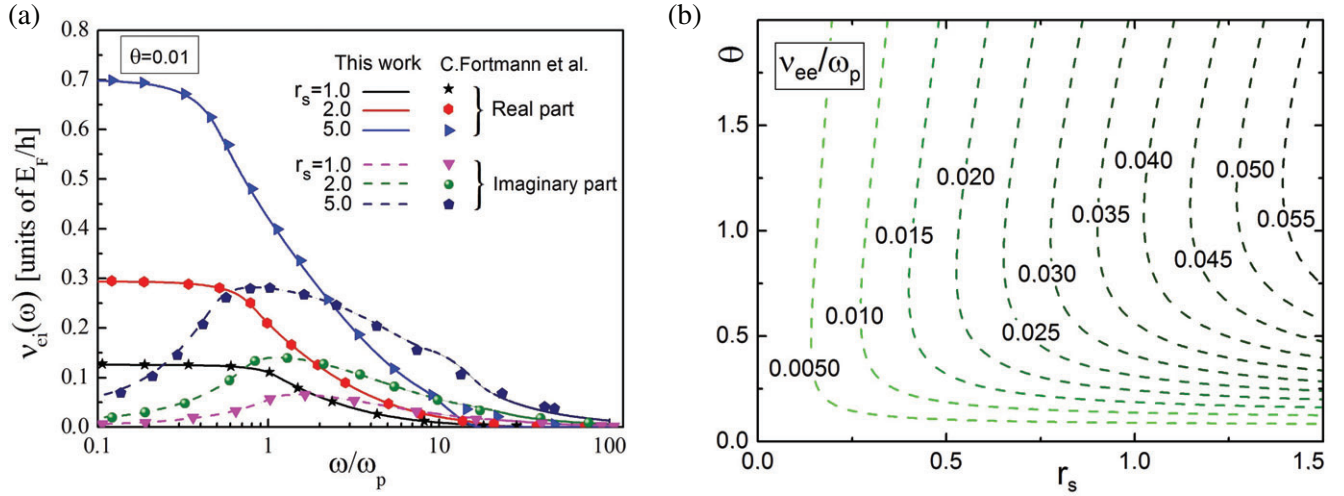

FIGURE 2 (a) Real and imaginary parts of the electron–ion dynamical collision frequency, Equation (5), at $\theta = 0.01$ for different values of r_s compared to results by Fortmann et al.[17] (symbols). (b) Electron–electron static collision frequency, Equation (6), for various values of θ and r_s

to both ν_{ei}^{RPA} and ν_{ei}^{LB}. Also, both ν_{ei}^{RPA} and ν_{ei}^{Y} essentially fail to correctly describe the general shape as well as the value of the imaginary part of ν_{ei}^{LB}. As will be shown below, the latter is critical for the correct computation of the dynamical ion potential.

Let us now discuss the contribution of e–e collisions to the total electronic collision frequency. For arbitrary degeneracy and in the Born approximation,[27] the parameterization for the static e–e collision frequency $\nu_{ee}(\omega = 0)$ reads[28]

$$\nu_{ee}(\omega = 0) = \frac{\nu_0}{\sqrt{1 + 0.2T/T_F}}, \tag{6}$$

where ν_0 is defined as

$$\nu_0 \equiv \nu_{ee}(\omega = 0; \theta \to 0) = \frac{3(k_B T)^2}{2\hbar m_e c^2} \sqrt{\frac{\alpha x^3}{\pi^3 (1 + x^2)^5/2}} \ J(y) \ ; \tag{7}$$

and $x = v_F/c$, $y = \sqrt{3}\hbar\widetilde{\omega}_p/k_B T$, and $\widetilde{\omega}_p = [4\pi e^2 n_e/(m_e(1 + x^2))]^{1/2}$. The function $J(y)$ has the form[29]

$$J(y) = \left[\frac{y^3}{3(1 + 0.07414y)^3} \times \ln\left(\frac{2.810}{y} - \frac{0.810x^2}{y(1 + x^2)} + 1 \right) \right.$$

$$\left. + \frac{\pi^5}{6} \frac{y^4}{(13.91 + y)^4} \right] \cdot \left(1 + \frac{6}{5x^2} + \frac{2}{5x^4} \right). \tag{8}$$

Equation (6) is applicable in the density range $1.4 \times 10^{-4} \leq r_s \leq 1.46$ (or equivalently $0.01 \leq x \leq 100$). The functional dependence of $\nu_{ee}(\omega = 0)$ on θ and r_s is shown in Figure 2b. It is seen that, with increasing r_s, $\nu_{ee}(\omega = 0)$ increases as the e–e coupling
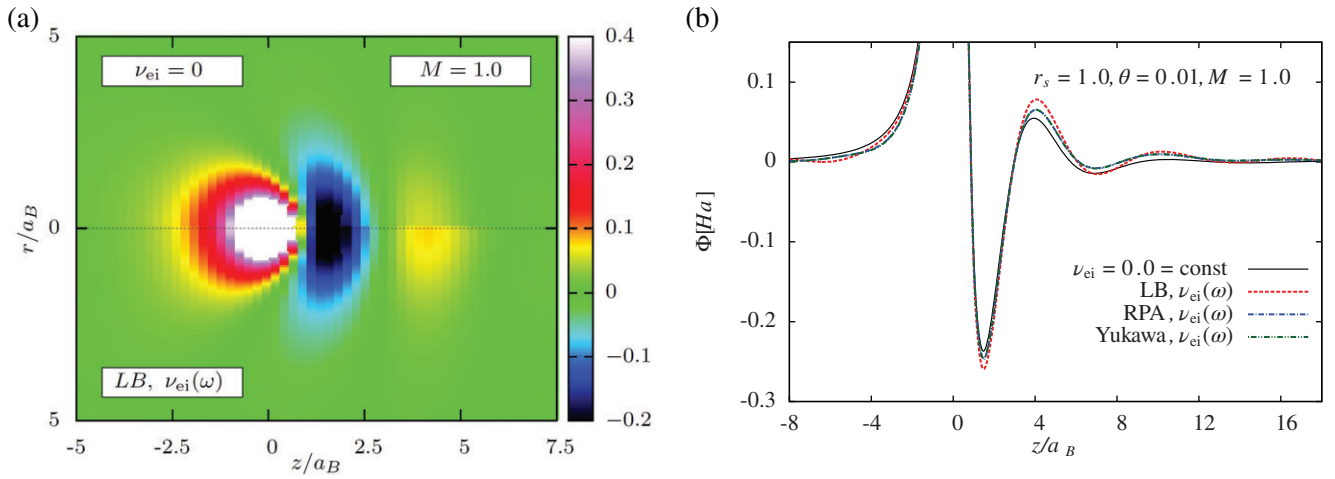
FIGURE 3 Dynamically screened ion potential for the sonic case, $M = 1$, at $r_s = 1$ and $\theta = 0.01$. In cylindrical coordinates, the electron streaming velocity relative to a resting ion (located at $r = 0$ and $z = 0$) is directed from left to right along the z-axis. In (a), the upper panel (indicated as $\nu_{ei} = 0$) is neglecting electronic collisions while in the lower panel (indicated as LB $\nu_{ei}(\omega)$) the Lenard–Balescu electron–ion collision frequency, Equation (3), is used. The right side (b) shows a section through the ion potential along the z-axis using Equation (3) (Lenard–Balescu [LB]), Equation (4) (random phase approximation [RPA]), Equation (5) (Y), as well as neglecting electronic collisions ($\nu_{ei} = 0$)

(correlations) becomes stronger. At $\theta \lesssim 1$, the temperature dependence is non-monotonic because of the interplay between Pauli blocking and thermal excitations.

Finally, let us consider the relevance of the e–e collisions: At $r_s = 1$, for $\theta = 1.0$ we have $\nu_{ei}^{LB}/\nu_{ee}|_{\omega=0} \approx 2.5$ and for $\theta = 0.01$ this ratio is substantially larger, $\nu_{ei}^{LB}/\nu_{ee}|_{\omega=0} \approx 30$. With decreasing temperature θ, Pauli blocking leads to a decrease of the e–e collision frequency. On the contrary, with temperature, the e–i collision frequency increases because of the stronger e–i coupling.

In the following, we investigate the particular effect of the frequency dependence of collisions on the dynamical screening by using $\nu_{ei}^{LB}(\omega)$. Therefore, we focus on the case of strong degeneracy ($\theta = 0.01$) and neglect the minor contribution of $\nu_{ee}(\omega)$. Note that the effect of thermal excitations on the wakefield around an ion was studied in detail in our previous works.[3,5] The general trend is that electronic thermal excitations lead to a reduction of the wake effects.[3] Detailed discussions of the nature of the e–e collisions in warm dense matter and related problems have been given by Reinholz et al.[30]

3 | DYNAMICALLY SCREENED ION POTENTIAL

The dynamically screened ion potential (1) is plotted in Figure 3 for the sonic case $M = 1$ at $r_s = 1$ and $\theta = 0.01$. The electronic streaming velocity relative to an immobile ion is directed from left to right along the z-axis. The ion is located at the origin ($r = 0$ and $z = 0$). The upper panel of the contour plot, Figure 3a, neglects electronic collisions, while the lower panel displays the ion potential taking into account $\nu_e = \nu_{ei}^{LB}(\omega)$. From Figure 3a, we can deduce that electronic collisions lead to a pronounced second maximum (located approximately at $z = 4a_B$). This effect is known as collision–induced amplification of the wakefield.[5] Therefore, for adequate description of the wakefield, the inclusion of collisions is important.

In Figure 3b, the ion potential along the z-axis is shown. Here we compare the results obtained using $\nu_{ei}^{LB}(\omega)$, $\nu_{ei}^{RPA}(\omega)$, $\nu_{ei}^{Y}(\omega)$, and the collisionless case. Figure 3b clearly shows that not only the collisionless case but also the $\nu_{ei}^{RPA}(\omega)$- and $\nu_{ei}^{Y}(\omega)$-based results (which are on top of each other) cannot be regarded as accurate approximations to the $\nu_{ei}^{LB}(\omega)$-based potential, as they have lower absolute values of the minima and maxima in the downstream direction ($z > 0$). The main reason for this observation is that $\nu_{ei}^{RPA}(\omega)$ and $\nu_{ei}^{Y}(\omega)$ essentially fail to describe the imaginary part of $\nu_{ei}^{LB}(\omega)$ (see Appendix for more details). Therefore, instead of the computationally much simpler models $\nu_{ei}^{RPA}(\omega)$ and $\nu_{ei}^{Y}(\omega)$, in the following the effect of dynamical collisions on the ion potential is considered on the basis of $\nu_{ei}^{LB}(\omega)$.

We recall that in the range $\omega < \omega_p$, the real part of the collision frequency $\nu_{ei}^{LB}(\omega)$ is almost constant and can be well approximated by a static collision frequency $\nu_{ei} = \nu_{ei}^{LB}(\omega = 0)$, see Figure 1. At larger frequencies, $\omega > \omega_p$, $\nu_{ei}^{LB}(\omega)$ strongly differs from the static collision frequency $\nu_{ei} = \nu_{ei}^{LB}(\omega = 0)$. In the same range, the imaginary part is small, but non-zero overall.

In order to analyse the effect of the frequency dependence of electronic collisions, we compare the results obtained using $\nu_{ei}^{LB}(\omega)$ with those computed using the static collision frequency $\nu_{ei}^{LB}(\omega = 0)$. Additionally, to evaluate the impact of the imaginary part in more detail, the LB data is also compared with the result obtained by neglecting the imaginary part of $\nu_{ei}^{LB}(\omega)$, i.e. assuming $\nu_{ei}^{LB}(\omega) = Re\, \nu_{ei}^{LB}(\omega)$ and $Im\, \nu_{ei}^{LB}(\omega) = 0$. For $M = 1$, the corresponding results are presented in Figure 4a,b at $r_s = 1$
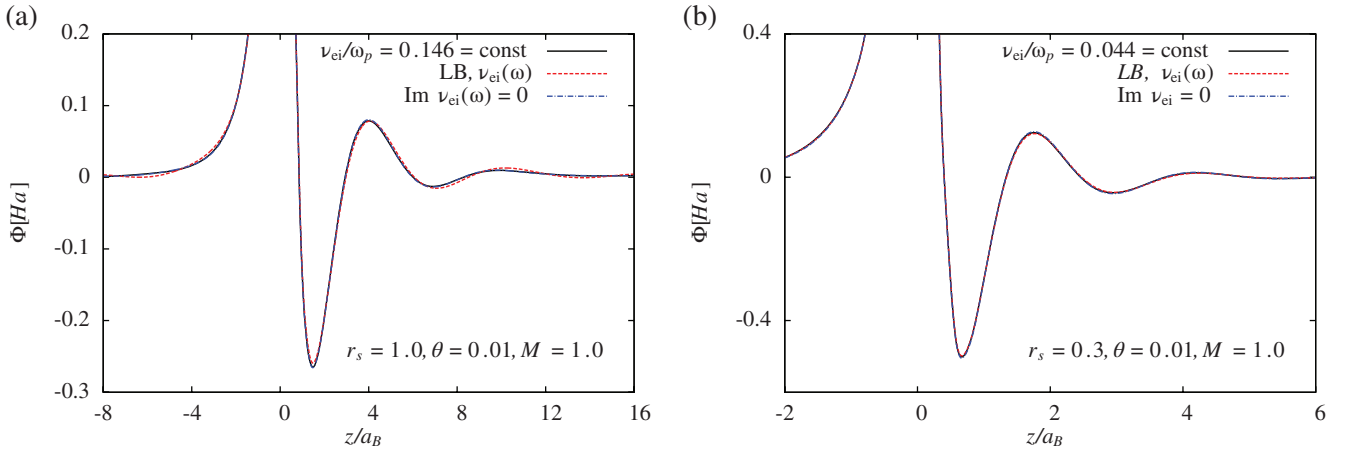
(a)

(b)

FIGURE 4   Dynamically screened ion potential for the sonic case, $M = 1$, at (a) $r_s = 1$ (see also the lower panel in Figure 3a), and (b) $r_s = 0.3$ using Lenard–Balescu, Equation (3), a static collision frequency $\nu_{ei} = \nu_{ei}^{LB}(\omega = 0)$, and neglecting the imaginary part of $\nu_{ei}^{LB}(\omega)$, i.e. $Im\ \nu_{ei}^{LB}(\omega) = 0$
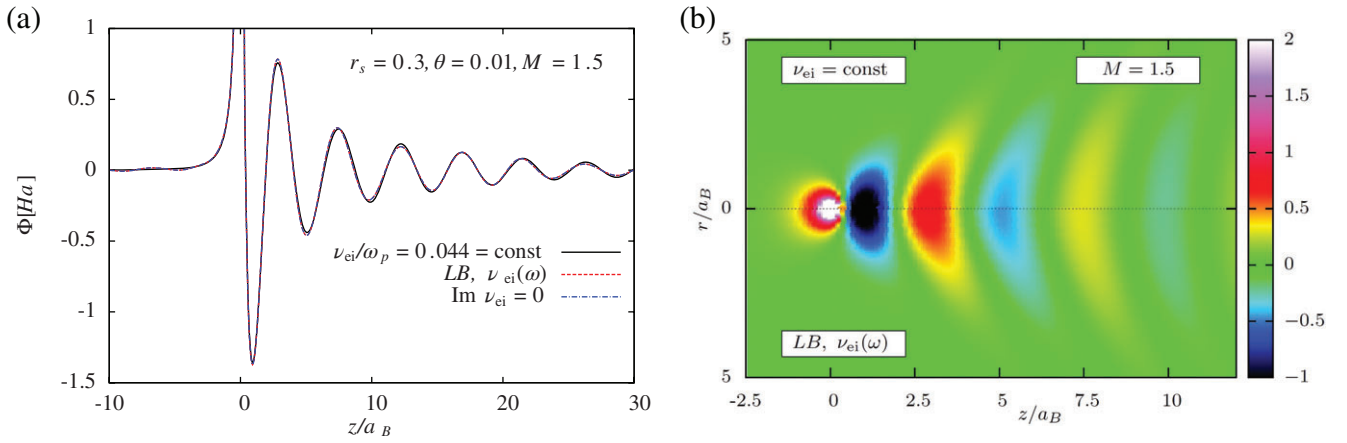
(a)

(b)

FIGURE 5   Dynamically screened ion potential for the super sonic case, $M = 1.5$, at $r_s = 0.3$ and $\theta = 0.01$. Left side (a) is for the same approximations as in Figure 4. In (b), the upper panel (indicated as $\nu_{ei} = const$) corresponds to a static collision frequency $\nu_{ei} = \nu_{ei}^{LB}(\omega = 0) = 0.044\omega_p$, while the lower panel (indicated as LB, $\nu_{ei}(\omega)$) corresponds to a dynamic electron–ion collision frequency, $\nu_{ei}^{LB}(\omega)$, given by Equation (3)

and $r_s = 0.3$, respectively. From these figures we see that the static collision frequency and the dynamic collision frequency give almost the same result. This means that the behaviour of $\nu_{ei}^{LB}(\omega)$ at $\omega > \omega_p$ (high energies) is not relevant to the formation of the wakefield. Indeed, from Figure 4 we see that neglecting the imaginary part of $\nu_{ei}^{LB}(\omega)$ makes no changes in the ion potential as well, since $Im\ \nu_{ei}^{LB}(\omega)$ is negligibly small in comparison to $Re\ \nu_{ei}^{LB}(\omega)$ at $\omega < \omega_p$, as discussed above.

Similar to the discussed sonic case, in the subsonic regime – where lower energy is deposited to induce the wakefield – it is also found that (i) the ion potential employing the approximation $\nu_{ei}^{RPA}(\omega)$ or $\nu_{ei}^{Y}(\omega)$ does not provide an accurate description of $\nu_{ei}^{LB}(\omega)$-based results, while (ii) the result computed using a static collision frequency $\nu_{ei}(\omega = 0)$ is in good agreement with that obtained by fully taking into account frequency-dependent collisions.

Finally, it is interesting to check whether the frequency dependence of electronic collisions is important in the supersonic case ($M > 1$). The results for this case are shown in Figure 5. In Figure 5a, the ion potential along the z-axis is presented for the same approximations as discussed in the sonic case. Additionally, the contour plot in Figure 5b shows the values of the ion potential on the ($r − z$) plane, where the upper panel corresponds to the case of a static collision frequency, $\nu_e = \nu_{ei}^{LB}(\omega = 0)$, while the lower panel shows the potential including a dynamical collision frequency, $\nu_e = \nu_{ei}^{LB}(\omega)$. From these figures, it is evident that the frequency dependence of the electronic collisions is not relevant in the considered supersonic case as well.

4 | CONCLUSION

The LB model for the dynamical e–i collision frequency was used to study the dynamical screening in dense plasmas at $r_s \leq 1$. It was shown that the dynamically screened ion potential is not sensitive to the energy (frequency) dependence of the electronic

collisions in the subsonic, sonic, and moderately supersonic cases. This means that the result for the static electronic collision frequency from other more accurate methods (e.g. the T-matrix approximation,[15,16,31] MD simulation,[10,32] or density functional theory[30]) can be used neglecting the frequency dependence, without loss of accuracy. This significantly reduces the complexity of the computation of the ion potential in streaming plasmas, e.g. in a time-dependent multi-scale modelling where the electronic dynamics are computed using quantum hydrodynamics[33,34] or by linear response theory,[19] and where the ions are treated by an MD simulation. Note that an effect related to the energy (frequency) dependence of the electronic collisions may manifest itself at very high values of the streaming velocity, $M \gg 1$, but the latter case is out of the scope of the present work and is left for future studies. Finally, we note that an alternative to include correlation effects in the electronic dielectric function is via local field corrections that can be obtained, for warm dense electrons, via quantum Monte Carlo simulations.[35,36]

ORCID

Zh.A. Moldabekov https://orcid.org/0000-0002-9725-9208

REFERENCES

[1] U. Zastrau, P. Sperling, M. Harmand, A. Becker, T. Bornath, R. Bredow, S. Dziarzhytski, T. Fennel, L. B. Fletcher, E. Förster, S. Göde, G. Gregori, V. Hilbert, D. Hochhaus, B. Holst, T. Laarmann, H. J. Lee, T. Ma, J. P. Mithen, R. Mitzner, C. D. Murphy, M. Nakatsutsumi, P. Neumayer, A. Przystawik, S. Roling, M. Schulz, B. Siemer, S. Skruszewicz, J. Tiggesbäumker, S. Toleikis, T. Tschentscher, T. White, M. Wöstmann, H. Zacharias, T. Döppner, S. H. Glenzer, R. Redmer, *Phys. Rev. Lett.* **2014**, *112*, 105002.
[2] B. Yu. Sharkov, D. H. H. Hoffmann, A. A. Golubev, Y. Zhao, *Matter Radiat. Extremes* **2016**, *1*, 28.
[3] Z. Moldabekov, P. Ludwig, M. Bonitz, T. Ramazanov, *Phys. Rev. E* **2015**, *91*, 023102.
[4] Zh. A. Moldabekov, P. Ludwig, J.-P. Joost, M. Bonitz, T. S. Ramazanov, *Contrib. Plasma Phys.* **2015**, *55*, 186.
[5] Zh. A. Moldabekov, P. Ludwig, M. Bonitz, T. S. Ramazanov, *Contrib. Plasma Phys.* **2016**, *56*, 442.
[6] N. D. Mermin, *Phys. Rev. B* **1970**, *1*, 2362.
[7] P. Ludwig, H. Jung, H. Kählert, J.-P. Joost, F. Greiner, Z. Moldabekov, J. Carstensen, S. Sundar, M. Bonitz, A. Piel, *Eur. Phys. J. D* **2018**, *72*, 82.
[8] R. I. Golyatina, S. A. Maiorov, *Phys. Sci. Technol.* **2017**, *4*, 4.
[9] M.-J. Lee, Y.-D. Jung, *Phys. Sci. Technol.* **2016**, *3*, 20.
[10] I. Morozov, H. Reinholz, G. Röpke, A. Wierling, G. Zwicknagel, *Phys. Rev. E* **2005**, *71*, 066408.
[11] H. Reinholz, *Phys. Part. Nucl.* **2008**, *39*, 998.
[12] H. Reinholz, Yu. Zaporoghets, V. Mintsev, V. Fortov, I. Morozov, G. Röpke, *Phys. Rev. E* **2003**, *68*, 036403.
[13] M. Veysman, G. Röpke, M. Winkel, H. Reinholz, *Phys. Rev. E* **2016**, *94*, 013203.
[14] P. Sperling, S. Rosmej, R. Bredow, L. B. Fletcher, E. Galtier, E. J. Gamboa, H. J. Lee, H. Reinholz, G. Röpke, U. Zastrau, S. H. Glenzer, *J. Phys. B: At. Mol. Opt. Phys.* **2017**, *50*, 134002.
[15] H. Reinholz, R. Redmer, G. Röpke, A. Wierling, *Phys. Rev. E* **2000**, *62*, 5648.
[16] A. Wierling, Th. Millat, G. Röpke, R. Redmer, *Phys. Plasmas* **2001**, *8*, 3810.
[17] C. Fortmann, A. Wierling, G. Röpke, *Phys. Rev. E* **2010**, *81*, 026405.
[18] R. Thiele, T. Bornath, C. Fortmann, A. Höll, R. Redmer, H. Reinholz, G. Röpke, A. Wierling, S. H. Glenzer, G. Gregori, *Phys. Rev. E* **2008**, *78*, 026411.
[19] P. Ludwig, M. Bonitz, H. Kählert, J. W. Dufty, *J. Phys.: Conf. Ser.* **2010**, *220*, 012003.
[20] P. Ludwig, C. Arran, M. Bonitz, in *Complex Plasmas: Scientific Challenges and Technological Opportunities* (Eds: M. Bonitz, J. Lopez, K. Becker, H. Thomsen), Springer International Publishing, Cham **2014**, p. 73.
[21] J. Lindhard, *Mat. Fys. Medd. Dan Vid. Selsk.* **1954**, *28*, 8.
[22] Zh. A. Moldabekov, S. Groth, T. Dornheim, H. Kählert, M. Bonitz, T. S. Ramazanov, *Phys. Rev. E* **2018**, *98*, 023207.
[23] H. Reinholz, G. Röpke, *Phys. Rev. E* **2012**, *85*, 036401.
[24] Zh. Moldabekov, T. Schoof, P. Ludwig, M. Bonitz, T. Ramazanov, *Phys. Plasmas* **2015**, *22*, 102104.
[25] D. Semkat, R. Redmer, T. Bornath, *Phys. Rev. E* **2006**, *73*, 066406.
[26] Wolfram Research, Inc., *MATHEMATICA, ver. 8.0*, Wolfram Research, Inc., Champaign, IL **2010**.
[27] M. Lampe, *Phys. Rev.* **1968**, *170*, 306.
[28] M. D. Barriga-Carrasco, A. Y. Potekhin, *Laser Part. Beams* **2006**, *24*, 553.
[29] A. Y. Potekhin, D. A. Baiko, P. Haensel, D. G. Yakovlev, *Astron. Astrophys.* **1999**, *346*, 345.
[30] H. Reinholz, G. Röpke, S. Rosmej, R. Redmer, *Phys. Rev. E* **2015**, *91*, 043105.
[31] N. Schlünzen, M. Bonitz, *Contrib. Plasma Phys.* **2016**, *56*, 5.
[32] T. S. Ramazanov, Zh. A. Moldabekov, *Phys. Sci. Technol.* **2015**, *2*, 53.
[33] Zh. Moldabekov, M. Bonitz, T. Ramazanov, *Phys. Plasmas* **2018**, *25*, 031903.
[34] D. Michta, F. Graziani, M. Bonitz, *Contrib. Plasma Phys.* **2015**, *55*, 437.
[35] S. Groth, T. Dornheim, T. Sjostrom, F. D. Malone, W. M. C. Foulkes, M. Bonitz, *Phys. Rev. Lett.* **2017**, *119*, 135001.
[36] T. Dornheim, S. Groth, M. Bonitz, *Phys. Rep.* **2018**, *744*, 1.

APPENDIX

In Figure A1 we present the dynamically screened ion potential obtained for $M = 1$, $r_s = 1$, and $\theta = 0.01$. In (a) and (b) we compare $\nu_{ei}^{RPA}(\omega)$- and $\nu_{ei}^{Y}(\omega)$-based potentials, respectively, with the corresponding static collision frequency approximation as well as the result neglecting the imaginary part of $\nu_{ei}(\omega)$, i.e. taking $\nu_{ei}(\omega) = \mathrm{Re}\ \nu_{ei}(\omega)$.

In contrast to the case with $\nu_{ei}^{LB}(\omega)$, in Figure A1 we see that the imaginary parts of $\nu_{ei}^{RPA}(\omega)$ and $\nu_{ei}^{Y}(\omega)$ have significant impact on the dynamical screening. As shown in Figure 1, both $\nu_{ei}^{RPA}(\omega)$ and $\nu_{ei}^{Y}(\omega)$, being approximations to the more accurate $\nu_{ei}^{LB}(\omega)$, significantly overestimate the imaginary part of the collision frequency at $\omega < \omega_p$ in comparison to $\nu_{ei}^{LB}(\omega)$. This discrepancy leads to lower absolute values of the dynamically screened potential compared to LB result, see Figure 3b. Indeed, in both parts of Figure A1, the potential with $Im\ \nu_{ei}^{RPA}(\omega) = 0$ (as well as $Im\ \nu_{ei}^{Y}(\omega) = 0$) are very close to the potential with the constant collision frequency, which, in turn, is a very good approximation of the potential with LB dynamical collision frequency, see Figure 4.
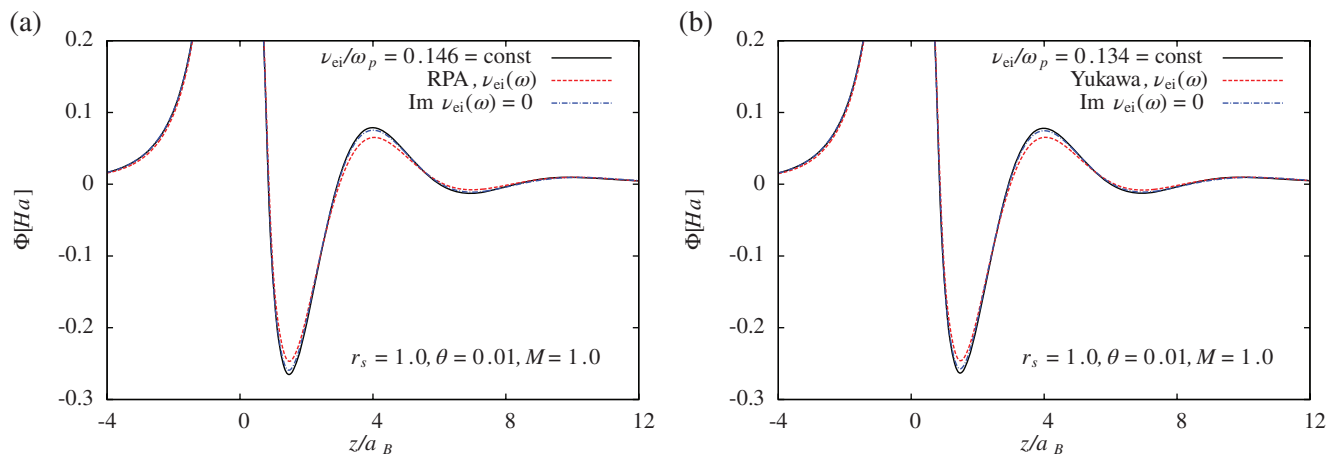
(a)

(b)

FIGURE A1 Dynamically screened ion potential obtained for $M = 1$ at $r_s = 1.0$ and $\theta = 0.01$, in analogy to Figure 4 but (a) for $\nu_{ei}^{RPA}(\omega)$, Equation (4), and (b) for $\nu_{ei}^{Y}(\omega)$, Equation (5)